Development of ruthenium oxide modified polyethersulfone membranes for improvement of antifouling performance including decomposition kinetic of polymer

Basak Yigit
Tarsus Üniversitesi: Tarsus Universitesi
Yasin Ozay
Tarsus Üniversitesi: Tarsus Universitesi
Fatih Mehmet Emen
Burdur Mehmet Akif Ersoy Üniversitesi: Burdur Mehmet Akif Ersoy Universitesi
Emine Ozsoy
Burdur Mehmet Akif Ersoy Üniversitesi: Burdur Mehmet Akif Ersoy Universitesi
Kasım Ocakoglu
Tarsus Üniversitesi: Tarsus Universitesi
Nadir Dizge (nadirdizge@gmail.com)
Mersin University: Mersin Universitesi

Research Article

Keywords: Ruthenium oxide, composite membrane, protein separation, flux recovery, decomposition kinetic of polymer

Posted Date: April 12th, 2022

DOI: https://doi.org/10.21203/rs.3.rs-1519358/v1

Abstract

In this study, RuO_2-embedded PES membrane was prepared and it was used for protein separation. The antifouling properties of the fabricated composite membranes were also investigated using bovine serum albumin (BSA) as protein solution. The mean roughness increased proportionally by introducing RuO_2 particles. The porosity of the composite membranes was higher than that of the pristine PES membrane. On the other hand, composite membranes has smaller average pore size after addition of RuO_2 particles. The blending of RuO_2 particles to the PES membrane caused to increase the hydrophilicity of the pristine membrane from 76.67° to 67.13°. The thermal studies of the PES/RuO_2 membranes were performed by DTA/TG. The Activation Energy (E_a) values of the PES/RuO_2 membranes were found to be 57.67-641.34 kJ/mol for Flynn-Wall-Ozawa (FWO) and 55.13–659.10 kJ/mol for Kissenger-Akahira-Sunose (KAS). The pure water flux of the composite membranes decreased from the pristine PES to PES/RuO_2 1.00 wt%. The pore size was calculated as 14.5 nm and pore size decreased up to 6.5 nm when blended RuO_2 particles increased up to 1.00 wt.%. BSA fluxes were 84.1 ± 2.1, 86.3 ± 2.5, and 93.9 ± 3.2 L/m^2/h for pristine, PES/RuO_2 0.50 wt%, and PES/RuO_2 0.75 wt% membranes, respectively. PES/RuO_2 1.00 wt%. membrane supplied the lowest BSA flux (73.6 ± 3.1 L/m^2/h). BSA rejection efficiencies increased from 45.5 ± 1.8% to 92.6 ± 1.5% when blended RuO_2 particles increased from 0 to 1.00 wt%. The results depicted that R_{ir} values decreased while R_r values increased after the blending of RuO_2.

1. Introduction

Industrial wastewater often contains hazardous macromolecules and environmentally unfriendly dyes. For this reason, permanent damages arising from the toxicity and carcinogenicity of many dyes in wastewater are significantly taken into consideration. Generally, three approaches are widely used to treat water and wastewater, including some treatments such as physical, chemical and biological [1]. Membranes are widely used in different industries such as medical, pharmaceutical, chemical, food and textile. In these days, membrane processes are used extensively to obtain water with high quality for domestic or industrial demands, purification and reuse of wastewater, and removal or recovery of valuable or toxic components from different industrial wastewaters [2]. Pressure-driven membrane process has gained great interest in several industrial activities such as textile, chemical, water softening, pharmaceutical, etc. [3][4].

Recent studies have been targeted on choosing a suitable polymer and adding an productive contribution to the structure of the membrane to evolve the properties of that membranes [4–6]. Polyethersulfone (PES) is well-known as one of the most practicable polymers in laboratory scale and field operations for the producing of polymeric membranes. The high thermal steadiness, well mechanical properties, and perfect heat-aging resistance of the PES polymer have motivated researchers to use it in several membrane processes [7]. However, the natural hydrophobicity of PES limits water flux permeability and the antifouling properties. To handle that problem, numerous metal oxide nano materials such as silver

[5], cobalt [6], iron oxide [7], alumina [8], titanium oxide [9] have attracted great attention as effective additives [8].

Ruthenium (IV) oxide (RuO_2) is an inorganic compound that is applied well done in different areas in chemistry such as in electrocatalysis and heterogeneous catalysis. Like most other platinum group metals, ruthenium is quite resistant to chemical reaction [10]. RuO_2 has some superior properties such as indissoluble structure in nature, adsorption capacity in pH range (3–11), and no explorable dissolution in the presence of 0.1 M HCl [11].

According to the best of our knowledge, there is no research paper has been published with RuO_2 blended PES membrane. Accordingly, we focused to produce a new mixed matrix membrane blended with RuO_2, to investigate the separation ability of the fabricated membranes against protein, and to measure the anti-fouling properties of membranes against BSA. Moreover, thermal analyses and decomposition kinetics of pristine PES and PES/RuO_2 blended composite membranes were also investigated.

2. Materials And Methods

2.1. Materials

Ruthenium oxide (RuO_2), bovine serum albumin (BSA, Mw: 66,000 g/mol) and N-methyl-2-pyrrolidone (NMP) were purchased from Merck Company (Germany). Polyethersulfone (PES Ultrason E6020P, Mw: 58,000 g/mol) was purchased from BASF Company (Germany).

2.2. Preparation of ruthenium oxide (RuO_2)-blended PES membranes

Phase inversion method has been used for preparing of pristine and ruthenium oxide-blended PES membranes, where NPM was used as the solvent. The detailed analysis can be found in elsewhere [12]. Table 1shows that the composition of casting solution.

Table 1
Composition of the prepared RuO_2-blended PES membranes.

Membrane	PES (wt.%)	NMP (wt.%)	RuO_2 (wt.%)
Pristine PES	14	86.00	0.00
0.50 wt% PES/RuO_2	14	85.95	0.05
0.75 wt% PES/RuO_2	14	85.25	0.75
1.00 wt% PES/RuO_2	14	85.00	1.00

2.3. Characterization of the prepared composite membranes

The gravimetric method is used for calculate the overall porosity (ε) and the mean pore radius (r_p) is calculated by the Guerout–Elford–Ferry equation [12].

The surface morphology of the PES membranes was investigated by scanning electron microscopy (SEM, FEI, Quanta 650 Field Emission SEM). Atomic force microscopy (AFM) was used to characterize the surface roughness properties of the prepared membranes. The AFM analyses were performed on an AFM microscope (Park System XE-100 SPM). The square shape pieces of the membranes (approximately 1 cm^2) were cut and scanned in the tapping mode in the air. The standard deviation of all the height values within the given area is used for calculating of the average of the surface roughness (R_a) value. Three different points were tested and the average values of R_a were given as result. The surface hydrophilicity of the fabricated membranes was carried out by water contact angle measurement (Attension Theta Lite). The TG/DTA curves were obtained via Seiko II TG/DTA 7200 Instrument. The system was set at 10°C/min heating and 100 mL/min N_2 gas flow rate. TG curves were obtained atdifferent heating rates (5, 10, and 15 ^oC/min). Kinetic analysis of the composite membranes were performed using these curves. Platinum crucible was used as a pan. Al_2O_3 was used as reference and the samples were weighed in the range of 5 to 10 mg.

2.4. Protein rejection studies of the membranes

A dead-end filtration system (Sterlitech, HP4750 Stirred Cell) was used to test the efficiency of the prepared membranes. The system was filled with the 100 mg/L of BSA solution which was prepared in Phosphate Buffer Solution (PBS, 50 mM, pH 7.4 ± 0.1) to prevent denaturation of protein. BSA was filtrated at 5 bar for 120 min. The protein concentration of the permeate (C_p) and the feed (C_f) were tested by the Lowry method [13].

Total fouling ratio (R_t), reversible fouling ratio (R_r), and irreversible fouling ratio (R_{ir}) were calculated by Eqs. (1)–(3), respectively [14]. Moreover, flux recovery ratio (FRR) was calculated by Eq. (4).

$$R_t\ (\%) = \left(1 - \frac{J_p}{J_{w,1}}\right) \times 100 \quad (1)$$

$$R_r\ (\%) = \left(\frac{J_{w,2} - J_p}{J_{w,1}}\right) \times 100 \quad (2)$$

$$R_{ir}\ (\%) = \left(\frac{J_{w,1} - J_{w,2}}{J_{w,1}} \right) \times 100 \quad (3)$$

$$FRR\ (\%) = \left(\frac{J_{w2}}{J_{w1}} \right) \times 100 \quad (4)$$

3. Results And Discussion

3.1. Physical characterization of RuO_2-blended PES membranes

The surface SEM micrographs of the fabricated membranes are shown in Fig. 1. A homogenous dispersion without significant agglomeration was obtained for the composite membranes containing lower RuO_2 particles. On the other hand, agglomeration of the RuO_2 particles was observed on the surface of PES/RuO_2 1.0 wt% composite membrane. The EDS mapping depicted that the RuO_2 powders were well-spread inside of the structure of PES membranes (Fig. 2).

AFM analyses of the fabricated composite membranes are shown in Fig. 3. Pristine membrane showed lower mean roughness compared to RuO_2 blended membranes (Table 2). The mean roughness increased proportionally by introducing RuO_2particles.

Table 2
Roughness parameters of the composite membranes.

Membrane type	R_{pv} (nm)	R_q (nm)	R_a (nm)	R_z (nm)
Pristine PES	36.072	7.313	5.864	31.803
RuO_2 0.50 wt%	57.491	6.557	4.283	26.651
RuO_2 0.75 wt%	70.199	16.618	14.152	59.442
RuO_2 1.00 wt%	77.926	16.560	13.648	66.843

The mean pore size and overall porosity of the membranes are presented in Table 3. The results showed that the porosity of the composite membranes was higher than that of the pristine PES membrane. It could be elucidated with some parameters such as thermodynamic and kinetic during the phase inversion process were affected by ruthenium and oxygen groups and it impressed the structure of the composite membranes. Pristine membranes have higher average pore size than composite membranes. When the dope solution becomes much viscous, it limits the expansion of pores. For this reason, average pore sizes of RuO_2 blended membranes were reduced. The blending of RuO_2particles to the PES

membrane increased the hydrophilicity of the pristine membrane (from 76.67° to 67.13°). This can be explain with increasing of water molecules affinity by affected from the oxygen groups which are polar functional.

Table 3
Mean pore size, contact angle and porosity, and of the pristine and RuO_2 blended PES membranes

Membrane type	Porosity (%)	Mean pore radius (nm)	Contact angle (°)
Pristine PES	56.83 ± 1.17	16.47 ± 0.35	76.67 ± 1.21
RuO_2 0.50 wt%	60.99 ± 1.35	15.63 ± 0.39	73.23 ± 0.84
RuO_2 0.75 wt%	64.20 ± 0.53	9.96 ± 0.36	70.28 ± 0.77
RuO_2 1.00 wt%	68.94 ± 0.39	6.05 ± 0.32	67.13 ± 0.80

3.2. Membrane performance

3.2.1. Pure water flux

The pure water flux of the fabricated membranes decreased from the pristine PES to PES/RuO_2 1.00 wt% (Fig. 4A). A decrease in the flux from 439.7 ± 20.5 L/m^2/h (for pristine membrane) to 379.3 ± 15.1 L/m^2/h (for PES/RuO_2 1.00 wt% membrane) could be explained as the agglomeration of RuO_2 particles in the structure of composite membranes and balking the pores which caused smaller pore-sized membrane. This result is consistent with the calculated membrane pore diameter shown in Table 3. The calculated pore size decreased from 16.47 nm to 6.05 nm when blended RuO_2 particles increased from 0 to 1.00 wt.%. However, BSA fluxes were 84.1 ± 2.1, 86.3 ± 2.5, and 93.9 ± 3.2 L/m^2/h for pristine, PES/RuO_2 0.50 wt%, PES/RuO_2 0.75 wt% membranes, respectively. PES/RuO_2 1.00 wt%. membrane supplied the lowest BSA flux (73.6 ± 3.1 L/m^2/h) (Fig. 4B). The BSA rejection capasity of the membranes was also tested (Fig. 4C). BSA rejection efficiencies increased from 45.5 ± 1.8% to 92.6 ± 1.5% when blended RuO_2 particles increased from 0 to 1.00 wt.%. Both higher hydrophilicity and the smaller pore size of the composite membranes improved BSA rejection.

3.2.2. Antifouling performance

The most critical flux decrease (80.9%) caused by BSA fouling was observed due to the highest R_t value of the pristine PES membrane (Fig. 5A). However, R_t values of the composite membranes decreased 79.2%, 76.1%, and 72.7% for PES/RuO_2 0.50, PES/RuO_2 0.75, and PES/RuO_2 1.00 wt.%, respectively. Additionaly, Rir values decreased while Rr values increased after blending of RuO_2 (Fig. 5A). Furthermore, FRR and R_r/R_{ir} ratios of the membranes are shown in Fig. 5B. The irreversible membrane fouling is displaced into reversible membrane fouling in the filtration process due to increase of R_r/R_{ir} ratio, which caused from incorporation of RuO_2 particles [15]. RuO_2 particles prevented irreversible BSA adsorption

into composite membranes in order to form a hydration layer close the membrane surface [16]. FRR values increased from 39.6% for pristine PES membrane to 85.9% for RuO_2 1.00 wt.% membrane.

3.3. Thermal analyses of PES/RuO_2 membranes

The temperature ranges of degradation processes, DTA peaks, weight losses (%), and the leaving moieties in degradation processes for each step are presented in Table 4.

Table 4
The TG/DTA results of the PES membrane

Stage	DTA Peak/°C	TG temp. range/°C	Mass loss/%		Evolved moiety
			Exper.	Theor.	
I	127	62–208	7.11	5.59	-54.35 HSO_3
II	520	208–573	47.68	47.32	-259C_6H_4, -95.83HSO_3
III	-	573–775	5.86	5.54	-28.49C_6H_4, -12.95HSO_3
Residue	-	775	39.35	41.55	-[$(C_6H_4)_{230.51}(HSO_3)_{95.87}$]

TG/DTG/DTA graphs of PES/RuO_2 membranes are presented in Fig. 6.

The TG curve of the PES membrane shows that the degradation occurs in three steps. Dehydration was monitored in the temperature range of 25 to 100 °C, and 2.78% mass loss is attributed to the water molecule leaving the PES membrane. The first degradation step was observed between 62 °C and 208 °C, with a weight loss of 7.11% (5.59%, Theoretically). 54.35 moles of - HSO_3 groups left the structure at the end of the first step. The second degradation step is observed between 208 °C and 573 °C, and at this step, the 259 moles -C_6H_4 groups and the 95.83 moles -HSO_3 groups leave the structure corresponding to the weight loss 47.68% (47.32%, Theoretically). The third step was observed between 573 °C and 775 °C. In this step, leaving of 28.49 moles -C_6H_4 and 12.95 moles -HSO_3 groups from the structure was observed with 5.86% weight loss (5.54%. Theoritically). The remaining degradation product has the formula [$(C_6H_4)_{230.51}(HSO_3)_{95.87}$] corresponding to a mass of 39.35% (theo. 41.55%).

The DTG graph shows the five-step degradation. It is seen that the second and third degradation steps overlap in the DTG curve. Since it is difficult to evaluate, the fourth and fifth degradation steps were considered as one step in accordance with the TG curve. The first degradation is observed between 62 °C and 208 °C and the second degradation step is observed between 286 °C and 579 °C. The third degradation takes place in the region between 578 °C and 778 °C. The maximum point of the strongest peak in the DTG graph gives the temperature at which degradation is fastest. The maximum degradation temperature is observed at 518 °C. Two endothermic and exothermic peaks were detected between 66 °C and 572 °C. These peaks were determined to be 66–180 °C, 409–515 °C, 515–572 °C, respectively. These

peaks correspond to the degradation steps in accordance with the TG curve. The proposed degradation mechanism is showed in Scheme 1.

3.4. Kinetic analysis

The E_a values of degradation steps for each α (conversion degree) was calculated via FWO and KAS methods. It was recommended by the ICTAC kinetic committee to set E_a values between 0.05 and 0.95 in increments of 0.05. The equations are presented in Equations 5 and 6.

FWO equation:

$$\ln\beta = \left[\frac{A.E_a}{R.g(\alpha)}\right] - 5.3305 - 1.05178\frac{E_a}{R}.\frac{1}{T} \quad (5)$$

and KAS equation:

$$\ln\frac{\beta}{T^2} = \left[\ln\frac{AR}{g(\alpha)E_a}\right] - \frac{E_a}{R}.\frac{1}{T} \quad (6)$$

where, A *is* the pre-exponential factor, β *is* heating rate, T *is* absolute temperature, g(α) is an unknown function of conversion, and R is gas constant.

According to these equations, ln β vs. 1/T (for FWO) and ln β/T^2 vs. 1/T (for KAS) graphs are straight lines. The E_a values are calculated from the slopes of these graphs. The E_a values of all decomposition steps are given in Figs. 5–7.

3.4.1. Dedradation kinetics of pristine PES membrane

The E_a-α graphs for the degradation stages of the PES membrane are presented in Fig. 7A-C. It was detected that in the first stage the values of E_a with α = 0.05 to 1.00 decreased very sharply in the range from 0.05 to 1.00. The E_a values calculated via the FWO and KAS equations for this stage are 66.15 kJ/mol and 59.60 kJ/mol, respectively. In the second stage for α between 0.05 and 4.00 the E_a values are increase sharply, and then rapidly decrease. The average E_a's were calculated to be 796.11 kJ/mol and 829.23 kJ/mol, respectively. In the third step for α between 0.05 and 0.60 the E_a values slowly decrease and beyond this point, it was observed to increase sharply. The average E_a values were found to be 158.53 kJ/mol and 150.70 kJ/mol, respectively. Irregular increases and decreases in E_a values due to the increase in alpha values show that all degradation steps have multi-step degradation kinetics. The E_a values of the PES membrane are given in Table 5.

3.4.2. Degradation kinetics of PES/RuO_2 0.50 wt% membrane

The E_a-α graphs for the PES/RuO_2 0.50 wt% membrane are given in Figs. 8(A-C). In the first stage, E_a values tend to decrease and increase irregularly in the range a = 0.05 and 0.4. Then these values gradually decrease. According to the FWO and KAS, the E_a values were calculated were 76.92 kJ/mol and 75.51 kJ/mol, respectively. In the second stage, E_a values tend to decrease and increase sharply between a = 0.05 and 0.2, then the values tend to decrease irregularly. According to the FWO and KAS methods, The average E_a values were calculated to be 321.57 kJ/mol and 331.96 kJ/mol, respectively. In the third stage, the E_a's increase irregularly between a = 0.05 and 1.0. The average Ea values were found to be 641.34 kJ/mol and 659.10 kJ/mol, respectively. The irregular increases and decreases observed in the E_a values indicate that there are multi-step decoposition in all steps. The E_a values of the PES/RuO_2 0.50 wt% membrane are given in Table 5

3.4.3. Degradation kinetics of PES/RuO_2 0.75 wt% membrane

The E_a-α graphs for the PES/RuO_2 0.75 wt% membrane are given in Figs. 9(A-C).

In the first stage, the values of the E_a decrease rapidly between a = 0.05 and 0.25 and increase slowly between α = 0.25 and 0.95, then rapidly decrease again. The E_a values were found to be 57.67 kJ/mol for FWO and 55.15 kJ/mol for KAS. In the second stage, The E_a values are increasing rapidly between α = 0.05 and 0.15. Then the E_a values tend to increase irregularly with the increase in the value of α. The average E_a values were calculated as 163.21 kJ/mol and 159.72 kJ/mol. In the third stage, E_a values increase regularly between a = 0.05 and 0.65 and then they decrease irregularly with increasing a value. The average E_a values were found to be 377.28 kJ/mol and 381.53 kJ/mol. The irregular increase and decrease observed in Ea values indicate that there is multistep degradation in all steps. The *Ea* values of the PES/RuO_2 0.75 wt% membrane are given in Table 5.

3.4.4. Degradation kinetic of PES/RuO_2 1.00 wt% membrane

The E_a-α graphs for the PES/RuO_2 1.00 wt% membrane are given in Figs. 10(A-C).

In the first step, the E_a values decreased between a = 0.05 and 0.15 and increased up to a = 0.4. Later, the E_a values kept mostly constant with the increase in a values. According to both methods (FWO and KAS), the E_a values were calculated 39.43 kJ/mol and 35.43 kJ/mol. In the second stage, The E_a values increased gradually between a = 0.05 and 0.90 and then tended to decrease. The E_a values were found to be 150.78 kJ/mol and 144.03 kJ/mol. In the third stage, The E_a values are almost constant between a = 0.05 and 0.60. it tended to increase after this point. The E_a values were found to be 147.35 kJ/mol and 139.35 kJ/mol. The irregular distribution of E_a values shows the tendency of multistep degradation at all steps. The E_a values of the PES/RuO_2 1.00 wt% membrane are showed in Table 5.

Table 5
The calculated E_a values of the PES membranes

Sample	Degradation Stages	FWO *Ea*/kJ mol^{-1}	KAS *Ea*/kJ mol^{-1}
PES membrane	I	62.15	59.60
	II	796.11	829.23
	III	158.53	150.70
PES/RuO_2 0.50 wt% membrane	I	76.92	75.51
	II	321.57	331.96
	III	641.34	659.10
PES/RuO_2 0.75 wt% membrane	I	57.67	55,13
	II	163.21	159.72
	III	377.28	381.53
PES/RuO_2 1.00 wt% membrane	I	39.43	35.43
	II	150.78	144.03
	III	147.35	139.35

4. Conclusions

In this study, RuO_2-embedded PES membranes were fabricated by phase-inverion method and used for separation of protein. BSA was used to perform of the antifouling characteristing of the prepared membranes. All membranes were characterized by AFM, SEM-EDS, mean pore size, contact angle and porosity. The porosity of the composite membranes increased while the pore size decreased. Moreover, hydrophilicity of the composite membranes also increased after RuO_2 was spreaded into the PES membrane. The thermal analysis studies of the PES/RuO_2 membranes were also carried out via DTA/TG combined system. The E_a values of the PES/RuO_2 membranes were calculated to be 57.67-641.34 kJ/mol for FWO and 55.13–659.10 kJ/mol for KAS.

The pure water flux of the composite membranes decreased compared to pristine PES. However, BSA fluxes increased when RuO_2 concentration increased up to 0.75 wt%. BSA rejection properties increased from 45.5 ± 1.8% to 92.6 ± 1.5% when blended RuO_2 particles increased from 0 to 1.00 wt.%. The composite membranes indicated good antifouling performance during BSA filtration. RuO_2-blended PES membrane can be used to decrease membrane fouling.

Declarations

Conflict of Interest Statement

The authors whose names are listed immediately below certify that they have NO affiliations with or involvement in any organization or entity with any financial interest (such as honoraria; educational grants; participation in speakers' bureaus; membership, employment, consultancies, stock ownership, or other equity interest; and expert testimony or patent-licensing arrangements), or non-financial interest (such as personal or professional relationships, affiliations, knowledge or beliefs) in the subject matter or materials discussed in this manuscript.

References

1. Crini G, Lichtfouse E (2019) Advantages and disadvantages of techniques used for wastewater treatment. Environ Chem Lett 17:145–155. doi:10.1007/s10311-018-0785-9
2. Drioli E, Stankiewicz AI, Macedonio F (2011) Membrane engineering in process intensification—An overview. J Memb Sci 380:1–8. doi:10.1016/j.memsci.2011.06.043
3. Van Der Bruggen B, Vandecasteele C, Van Gestel T, Doyen W, Leysen R (2003) A review of pressure-driven membrane processes in wastewater treatment and drinking water production. Environ Prog 22:46–56. doi:10.1002/ep.670220116
4. ., 1. Pressure-driven membrane processes, in: Membr. Eng, De Gruyter (2018) : pp. 1–32. doi:10.1515/9783110281392-001
5. Rehan Z, Gzara L, Khan S, Alamry K, El-Shahawi MS, Albeirutty M, Figoli A, Drioli E, Asiri A (2016) Synthesis and Characterization of Silver Nanoparticles-Filled Polyethersulfone Membranes for Antibacterial and Anti-Biofouling Application, Recent Pat. Nanotechnol 10:231–251. doi:10.2174/1872210510666160429145228
6. Gzara L, Ahmad Rehan Z, Khan SB, Alamry KA, Albeirutty MH, El-Shahawi MS, Rashid MI, Figoli A, Drioli E, Asiri AM (2016) Preparation and characterization of PES-cobalt nanocomposite membranes with enhanced anti-fouling properties and performances. J Taiwan Inst Chem Eng 65:405–419. doi:10.1016/j.jtice.2016.04.012
7. Rowley J, Abu-Zahra NH (2019) Synthesis and characterization of polyethersulfone membranes impregnated with (3-aminopropyltriethoxysilane) APTES-Fe3O4 nanoparticles for As(V) removal from water. J Environ Chem Eng 7:102875. doi:10.1016/j.jece.2018.102875
8. Gohari B, Abu-Zahra N (2018) Polyethersulfone Membranes Prepared with 3-Aminopropyltriethoxysilane Modified Alumina Nanoparticles for Cu(II) Removal from Water. ACS Omega 3:10154–10162. doi:10.1021/acsomega.8b01024
9. Pakdel Mojdehi A, Pourafshari Chenar M, Namvar-Mahboub M, Eftekhari M (2019) Development of PES/polyaniline-modified TiO2 adsorptive membrane for copper removal. Colloids Surf Physicochem Eng Asp 583:123931. doi:10.1016/j.colsurfa.2019.123931

10. Over H (2012) Surface Chemistry of Ruthenium Dioxide in Heterogeneous Catalysis and Electrocatalysis: From Fundamental to Applied Research. Chem Rev 112:3356–3426. doi:10.1021/cr200247n
11. Luxton TP, Eick MJ, Scheckel KG (2011) Characterization and dissolution properties of ruthenium oxides. J Colloid Interface Sci 359:30–39. doi:10.1016/j.jcis.2011.03.075
12. Ocakoglu K, Dizge N, Colak SG, Ozay Y, Bilici Z, Yalcin MS, Ozdemir S, Yatmaz HC (2021) Polyethersulfone membranes modified with CZTS nanoparticles for protein and dye separation: Improvement of antifouling and self-cleaning performance. Colloids Surf Physicochem Eng Asp 616:126230. doi:10.1016/j.colsurfa.2021.126230
13. Lowry LP, Assay (1951)J. Biol. Chem.
14. Zinadini S, Rostami S, Vatanpour V, Jalilian E (2017) Preparation of antibiofouling polyethersulfone mixed matrix NF membrane using photocatalytic activity of ZnO/MWCNTs nanocomposite. J Memb Sci 529:133–141. doi:10.1016/j.memsci.2017.01.047
15. Shen X, Xie T, Wang J, Liu P, Wang F (2017) An anti-fouling poly(vinylidene fluoride) hybrid membrane blended with functionalized ZrO 2 nanoparticles for efficient oil/water separation. RSC Adv 7:5262–5271. doi:10.1039/C6RA26651G
16. Russell BA, Kubiak-Ossowska K, Mulheran PA, Birch DJS, Chen Y (2015) Locating the nucleation sites for protein encapsulated gold nanoclusters: a molecular dynamics and fluorescence study. Phys Chem Chem Phys 17:21935–21941. doi:10.1039/C5CP02380G

Scheme

Schemes 1 is available in the Supplementary Files section.

Figures

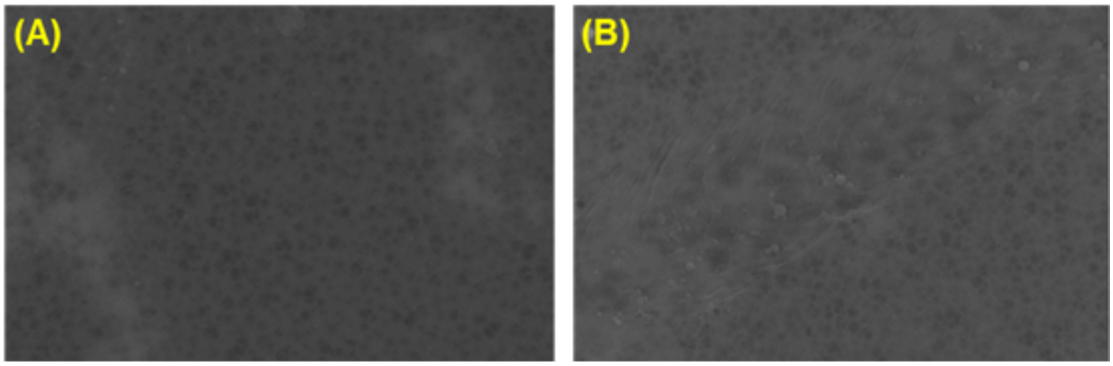

Figure 1

Top surface SEM images of composite membranes in different loading particles. **(A)** pristine PES, **(B)** PES/RuO_2 0.50 wt% **(C)** PES/RuO_2 0.75 wt% **(D)** PES/RuO_2 1.00 wt%.

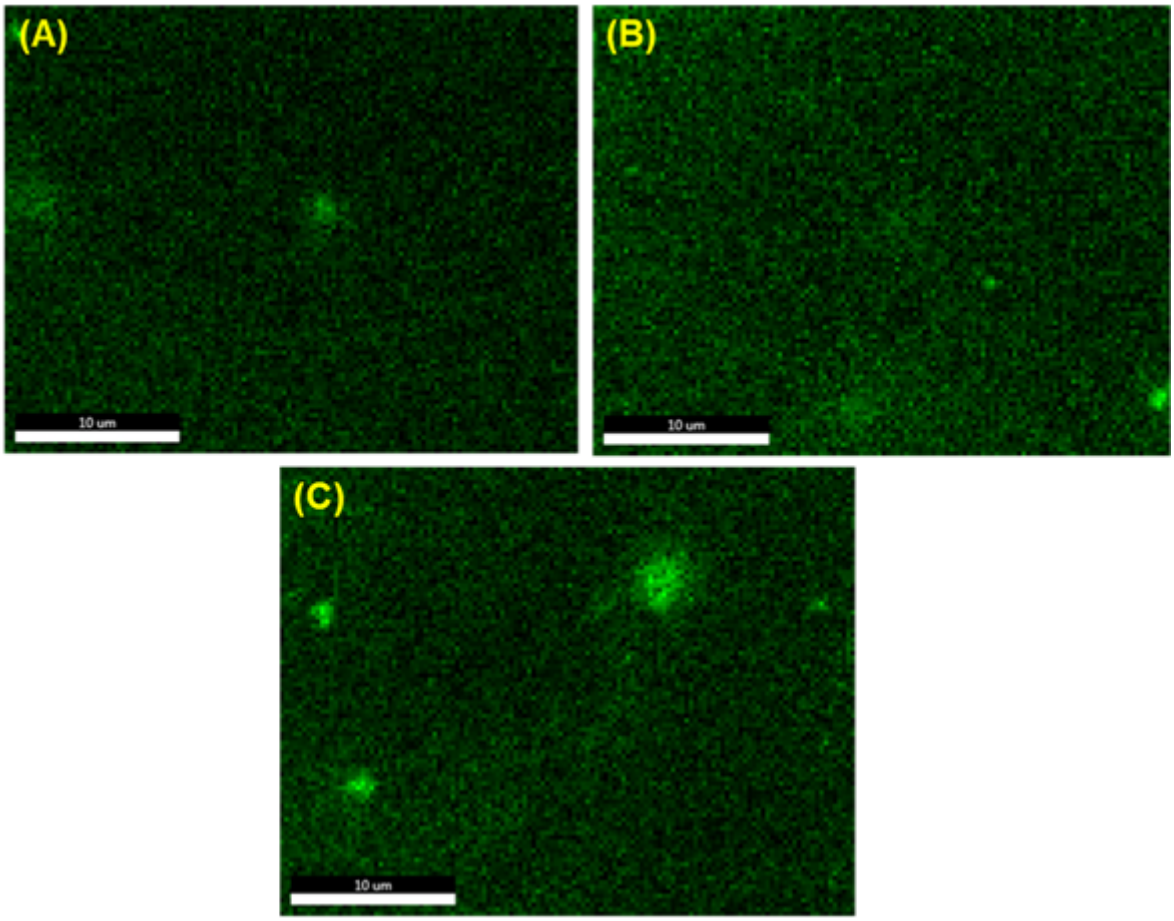

Figure 2

The EDS mapping of composite membranes in different loading of RuO_2 particles **(A)** PES/RuO_2 0.50 wt% **(B)** PES/RuO_2 0.75 wt% **(C)** PES/RuO_2 1.00 wt%.

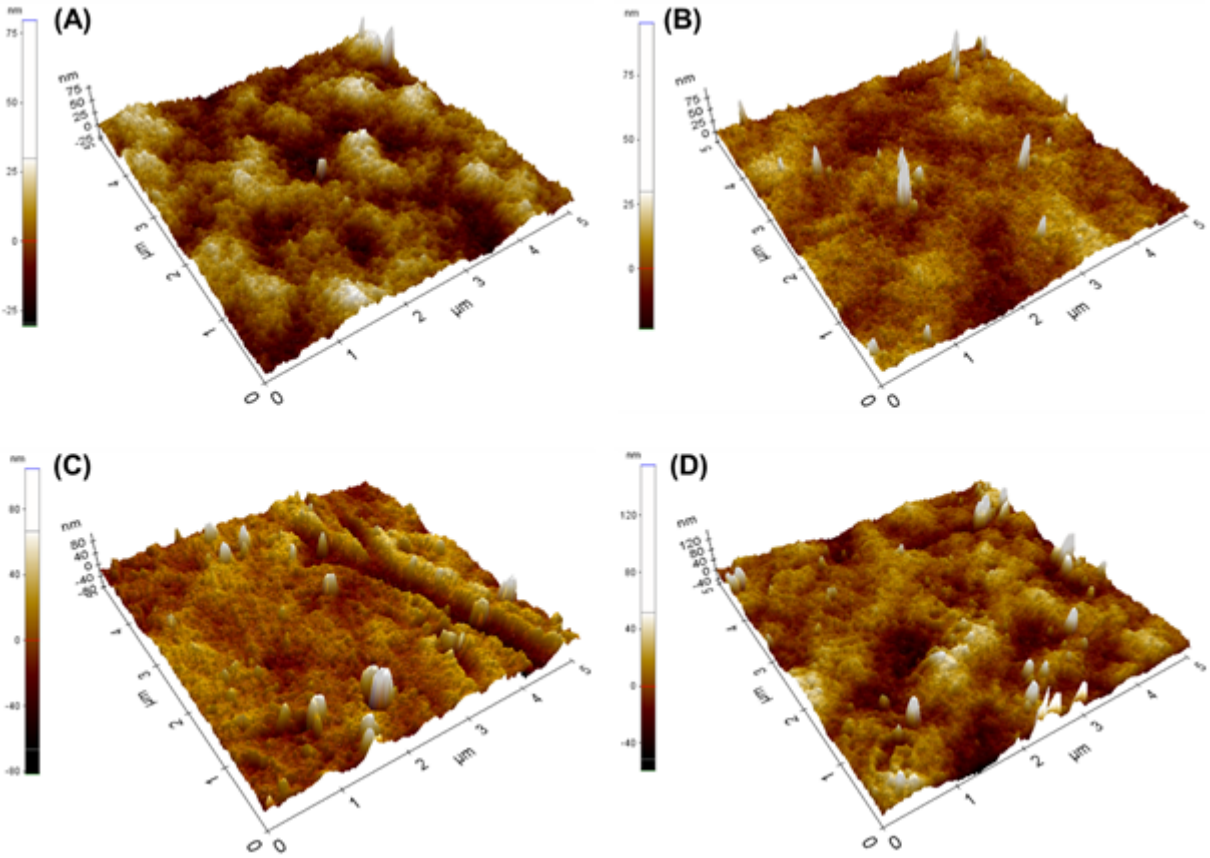

Figure 3

AFM analyses of composite membranes in different loading particles **(A)** pristine PES, **(B)** PES/RuO_2 0.50 wt% **(C)** PES/RuO_2 0.75 wt% **(D)** PES/RuO_2 1.00 wt%.

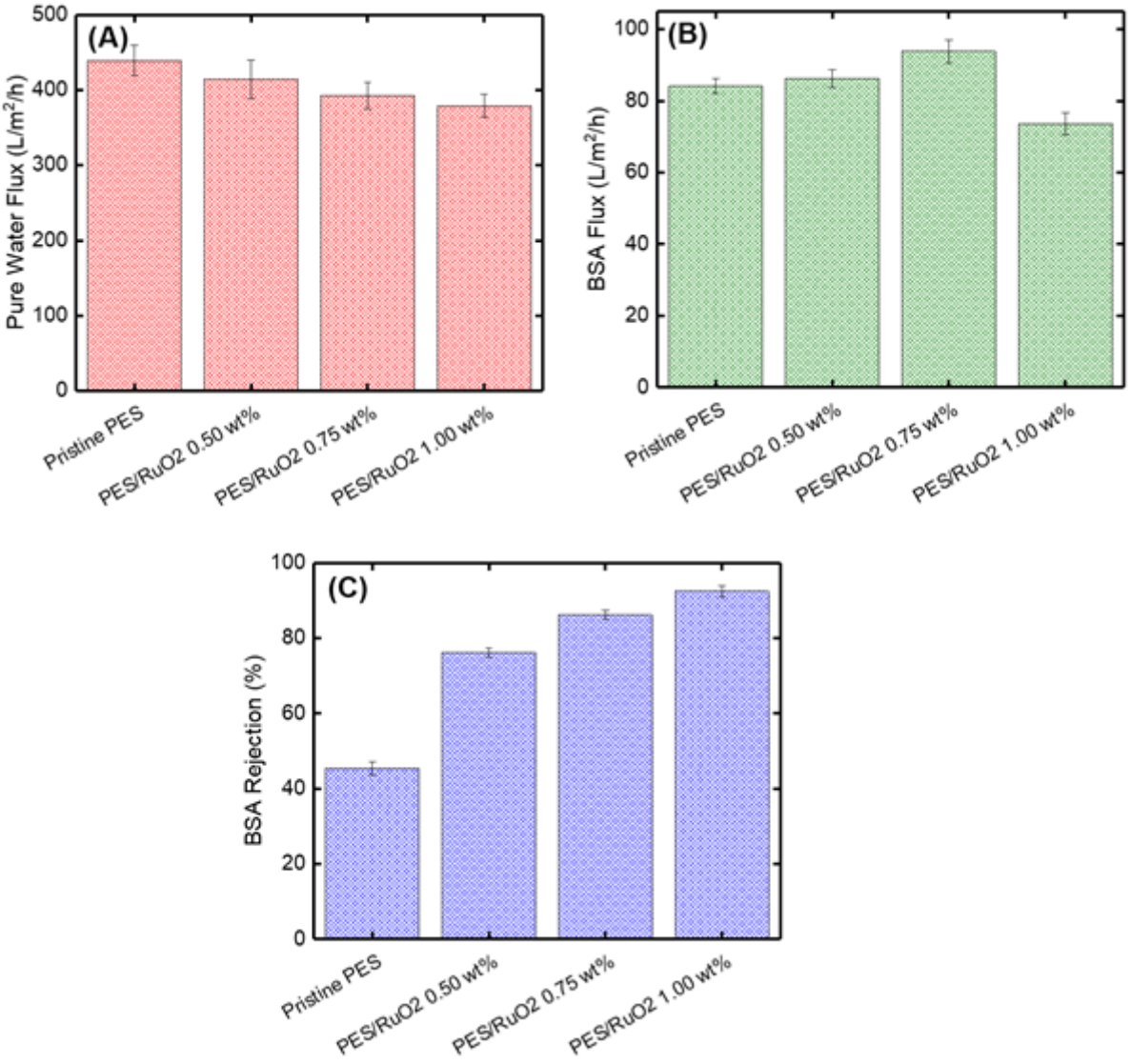

Figure 4

The performance of RuO_2-blended composite membranes **(A)** pure water flux, **(B)** BSA solution flux, and **(C)** BSA rejection.

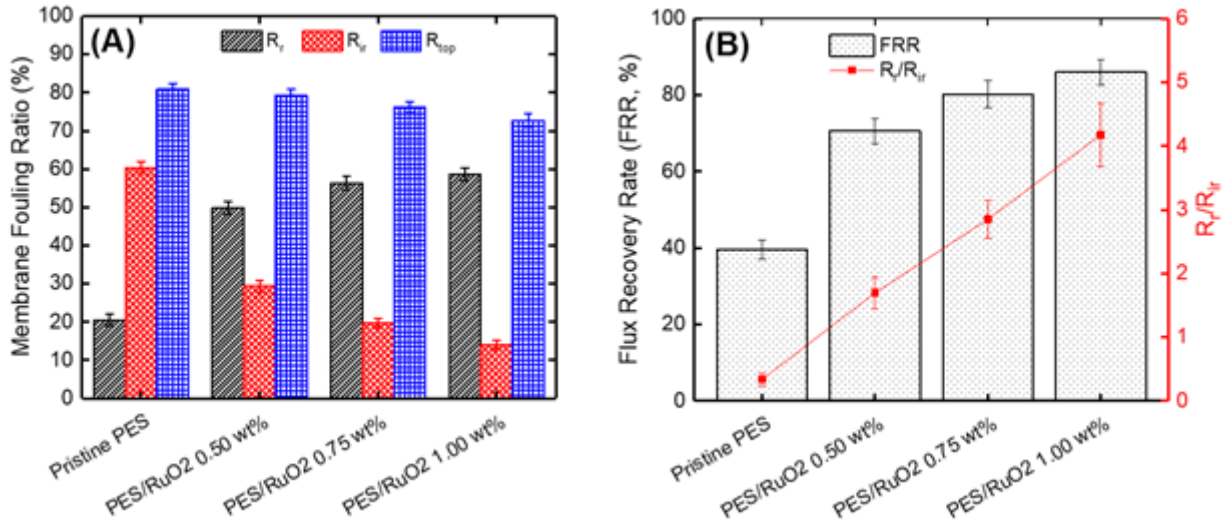

Figure 5

(A) R_r, R_r, and R_t fouling ratios and **(B)** FRR and R_r/R_{ir} ratios of pristine PES membrane and RuO_2-blended membranes.

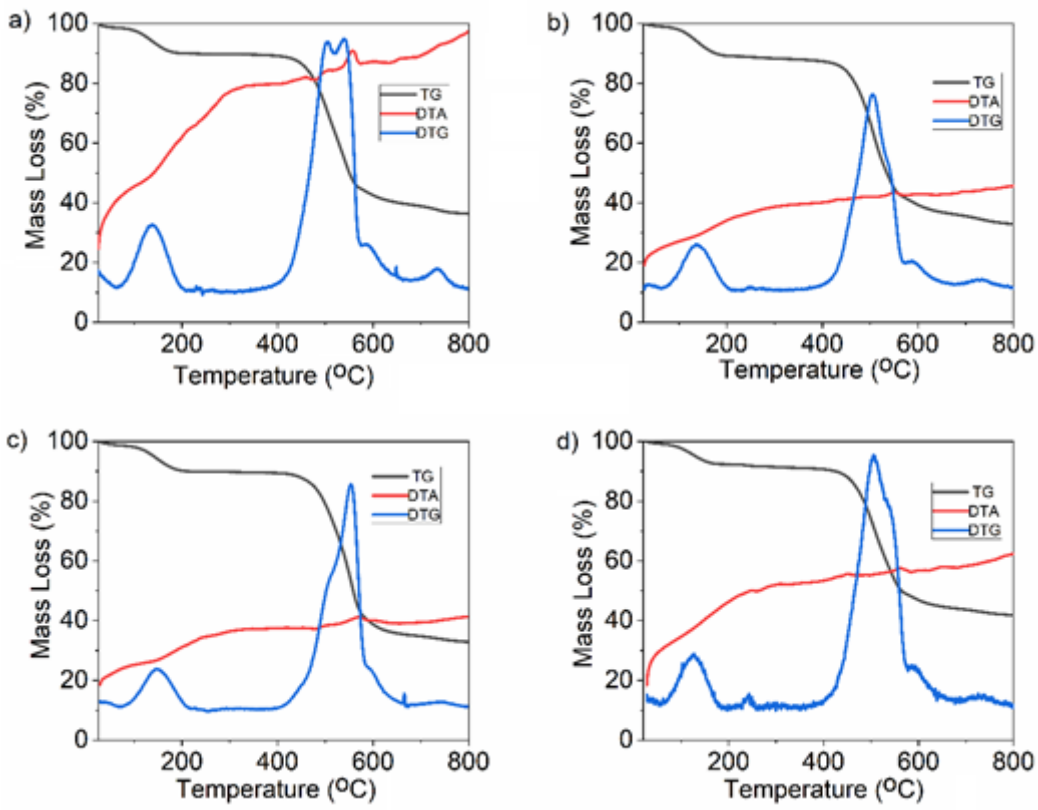

Figure 6

TG/DTG/DTA graphs of the pristine and PES/RuO_2 composite membranes **(A)** pristine PES, **(B)** PES/RuO_2 0.50 wt% **(C)** PES/RuO_2 0.75 wt% **(D)** PES/RuO_2 1.00 wt%.

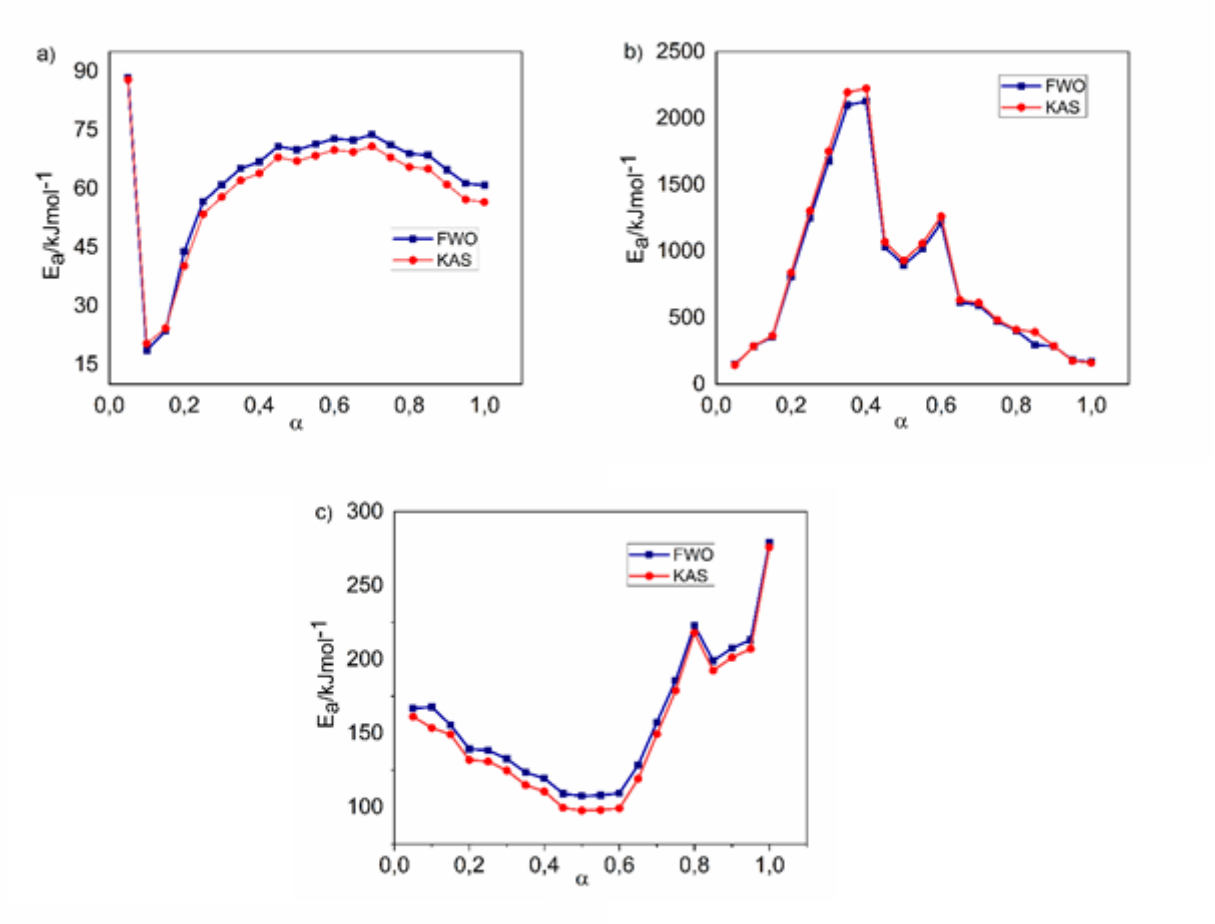

Figure 7

Ea-α plots of the PES membrane **(A)** the first degradation step **(B)** the second degradation step **(C)** the third degradation step.

Figure 8

Ea-α plots of the PES/RuO_2 0.50 wt% membrane **(A)** the first degradation step **(B)** the second degradation step **(C)** the third degradation step.

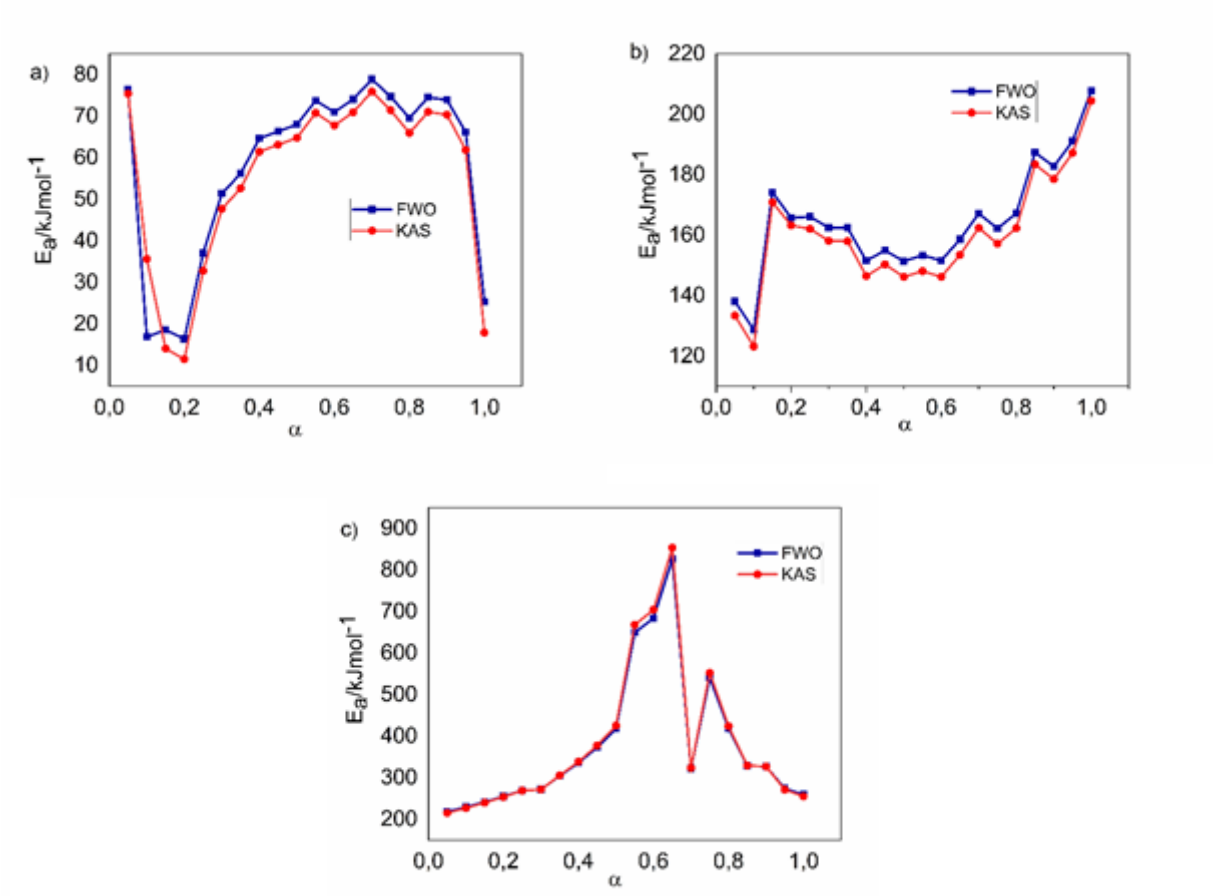

Figure 9

Ea-α plots of the PES/RuO_2 0.75 wt% membrane **(A)** the first degradation step **(B)** the second degradation step **(C)** the third degradation step.

Figure 10

Ea-α plots of the PES/RuO_2 1.00 wt% membrane **(A)** the first degradation step **(B)** the second degradation step **(C)** the third degradation step.

Supplementary Files

This is a list of supplementary files associated with this preprint. Click to download.

- Scheme1.png